Available online at www.sciencedirect.com

ScienceDirect

Procedia CIRP 100 (2021) 151–156

www.elsevier.com/locate/procedia

31st CIRP Design Conference 2021 (CIRP Design 2021)

Active control of blankholder in sheet metal stamping

M. Brun[a,*], A. Ghiotti[a], S. Bruschi[a], S. Filippi[b]

[a]*University of Padova, Department of Industrial Engineering, Via Venezia 1, 35131, Padova, Italy*
[b]*Extraflame S.p.A., Via Artigianato 12, 36030, Montecchio Precalcino, Italy*

* Corresponding author. Tel.: +39 049 8276816; *E-mail address:* michele.brun@phd.unipd.it

Abstract

The continuous demand of shape complexity, product accuracy and extended tools life has led to a widespread use of auxiliary systems in sheet metal stamping. Nevertheless, their performances are often inadequate, making their use a compromise between process efficiency and stability. The paper focuses on a new magneto-rheological actuator design. Both analytical and numerical approaches are developed to evaluate load response and to optimize the magnetic field interaction. A physical prototype according to the design outputs is manufactured and tested at different dynamic conditions. Finally, magnetic force values obtained from FE model and experimental tests are compared.

Keywords: Sheet Metal Forming; Stamping; Dies; Blankholder; Magnetorheological fluid

1. Introduction

In the last decades sheet metal forming industry has faced increasing requirements in terms of high accuracy, reduction of esthetic defects as well as the need of high productivity especially for automotive and mechanical sectors. Many improvements have been represented by auxiliary systems developed for blank holding or metal sheet flow control, i.e. the use of gas springs [1], independent hydraulic actuators and controlled die cushions in metal forming presses [2], [3], segmented blankholder [4], shock absorbers [5] (as reported in Fig. 1), all having the common purpose of increased accuracy of load application as well as higher flexibility in settings the process parameters to adapt the operating conditions to different production scenarios [6].

Flexibility, sensor fusion and Artificial Intelligence (AI) applications are the top trends that can be identified in the scientific and industrial literature of the last decade. Li et al. [7] investigated experimentally the applicability of active draw bead in sheet metal drawing. By using multiple draw bead trajectories, it was found that draw depth at fracture can be significantly improved and more efficient control of the drawing force compared traditional solutions. An active control system, capable of controlling the blankholder force distribution, was developed by Tommerup et al. [8]. The material flow was investigated for different process conditions showing that both geometry and thickness strain distribution of final part can be affected by the active system applied load. In [9] the research was exploited with the integration of a feedback control system to modulate both blankholder force distribution and magnitude. Experimental results showed that such control system can eliminate process instabilities, avoiding sheet tearing appearance on the stamped part.

Bäume et al. [10], [11] integrated piezo-electric actuators in deep drawing tool to redistribute the blankholder pressure. Optical sensors based on laser triangulation were used to monitor flange drawn-in during the process. The signals collected from the laser sensors were processed to control the action of piezo-electric actuators on the stamped part, resulting in higher product quality and reduce occurrence of defects or cracks on the stamped part. Barthau et al. [4] designed an experimental tool equipped with segmented blankholder (up to ten elastic segments), each moved by independent hydraulic actuators and servo-valves in order to locally apply different blank holding forces. Industrial piezo-electric sensors were mounted on the tool wall, to measure part wall stress during

10.1016/j.procir.2021.05.079

deformation and used to control hydraulic pistons pressure. Close-loop control algorithm was calibrated through both theoretical and numerical approaches and it was demonstrated an increase of process robustness and maximum drawing depth.

Sensors and tool integration were the focus of several studies, with the aim to realize in-line process monitoring and improve process control. Linear Variable Differential Transducers (LVDT) were successfully used in deep drawing for wrinkle height measuring [12], but the requirement to maintain physical contact between probe and workpiece during process was found to be the major limitation. To overcome such limitation contactless sensors have been developed. Sensing methods based on mutual inductance allowed measuring sheet draw-in during process [13] while eddy current sensors were integrated in the tooling support to detect spring backs of complex body car parts [14]. In [13] commercial piezo-resistive thin-film force sensors were evaluated to develop spatially continuous pressure profiles from discrete measurements. The pressure values at random location could be estimated with an error of less than 10%, and the binder force, evaluated by integration, have an error lower than 4%. A different technique for measuring the pressure map over the punch surface, based on discrete pressure measurements and numerical interpolation, was proposed in [15]. An example of this approach was presented by Groche et al. in [16], where the authors proposed a sensor fastener, which incorporated three strain gauges and a temperature probe, for process load measuring. The simple shape and the small size allowed its installation closed to the actual process, enabling economical measurements.

The introduction of smart fluids is dated about twenty year ago with the first application od Magneto-Rheological (MR) fluids. Yang et al. [17] presented a MR fluid damper for structural vibration reduction and anti-seismic application, providing an insight into MR fluid flow analysis, geometrical design considerations, electromagnetic circuit schematization and analytical formulations for evaluating MR damper load components. Despite the analytical formulations developed in several researches, to improve the MR devices performances the design phase has to be supported with FE tools to study the electromagnetic phenomena arising in the actuator and their interaction with the MR fluid [18]. Lam et al. [19] developed a MR damper with embedded force and displacement sensors. Experimental tests investigated the damper load response for different excitation input currents and the capability of the device for structural vibration closed-loop control. MR devices are not applied only to vibration control, but are also used to realize automotive components, as semi-active suspensions systems [20], [21] brakes [22], [23] and clutches [24], [25]. Regarding sheet metal forming processes, MR dampers are successfully implemented by Ghiotti et al. for the reduction of reverse load effect in blanking [26] and to improve the shear surface quality of the stamped parts [27].

The work described in the paper is part of a wide research framework that is aimed at developing a new concept of closed-loop control blank holding systems for sheet metal stamping based on (i) real-time controllable actuators that can be tuned over the process, (ii) innovative sensors to collect the process parameters and (iii) analytical and numerical algorithms for the data computation. The focus of the paper is on a new Magneto-Rheological (MR) actuator design that combines the effect of smart fluids and high-pressure gas in a compact and efficient design. In the first part, the design of the active control for the blankholder is introduced. Then, the innovative MR device that was designed and developed within the project is described, with the evaluation of the main performances. Finally, the main conclusions are reported.

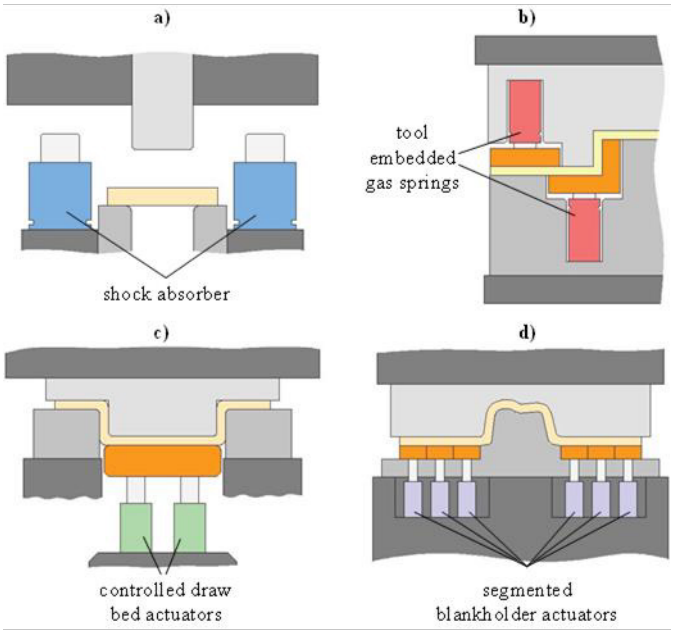

Fig. 1. Examples of auxiliary systems: a) hydraulic shock absorber for blanking; b) tool embedded gas springs; c) controlled draw bed for deep drawing; d) segmented blankholder.

2. Modelling blankholder active control

Sheet metal stamping processes operate in uncertain conditions with respect of mechanical properties of incoming material, interface conditions, forming machines characteristics and this often results in a critical control of defects (i.e. tearing, wrinkling, etc.) and part quality. Today, the major trend is represented by tentative to set active controls

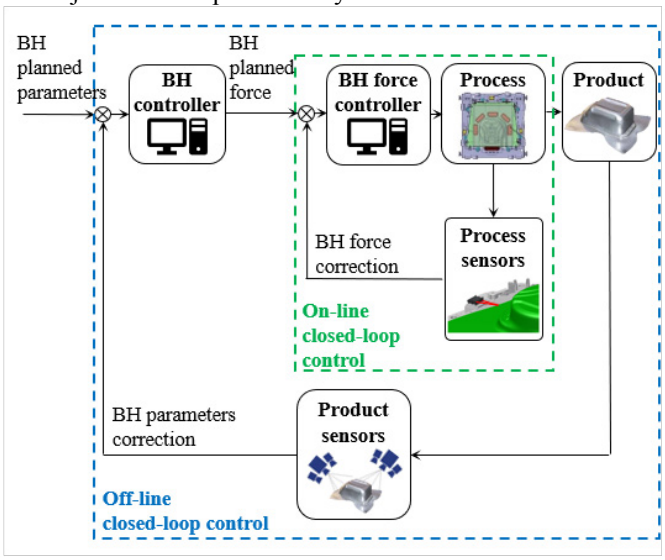

Fig. 2. On-line and off-line closed-loop control for blankholder force.

of the process parameters to rapidly adjust the dies configuration with respect to the external disturbs. The solution proposed in the paper is based on the use of MR fluid-based devices embedded within the blankholder to adjust the pressure by using a closed-control approach. This is possible thanks to the rapid change of viscosity that can be activated thanks to a magnetic field with a response time of few milliseconds. Moreover, the force generated by the devices can be modulated in respect of the magnitude of the applied magnetic fields, by varying the input current of the electromagnetic circuit.

The proposed in-line closed-loop control of the blankholder pressure is based on the possibility of varying the force of each MR actuator according to the sensor measurements performed directly on the stamped sheet, i.e. by means of laser sensors for material flow monitoring. Furthermore, this control logic can be extended to measurements performed on the final workpiece. As reported in Fig. 2, the first on-line closed-loop control allows adjustment during the production of a part, while the latter (off-line closed-loop control) permits adjustments only between different parts in the same batch.

As first step of the research, the design and the validation of an innovative MR actuator for sheet metal blank holding is presented. A new configuration is proposed that allows a compact design suitable for easy embedding in the blankholder structure and elevated force with respect to the small dimensions. A 2D electromagnetic FE model was developed in Ansys Maxwell® environment to reproduce the interaction between the MR fluid and magnetic field. From the results of the numerical simulations controllable load response was estimated by means the analytical formulations. Finally, experimental tests were conducted to evaluate the manufactured prototype performance at different speeds typical of the reference industrial processes.

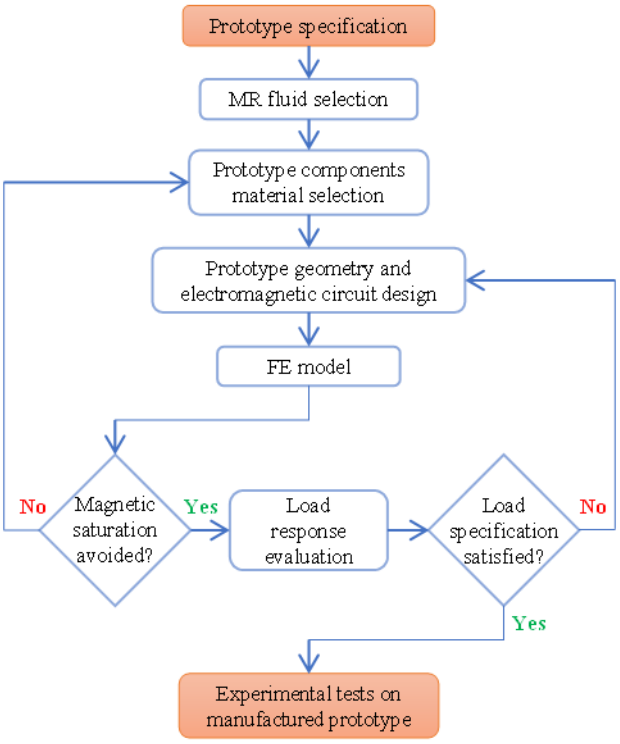

Fig. 3. Flowchart of the design stages.

3. Design of MR actuators

3.1. Design stages

Fig. 3 presents the flowchart of the design procedure followed in the design of the innovative MR actuator. At first stage, as target specifications, a stroke of 75 mm and a total force of 50 kN are chosen.

The selected MR fluid can be modelled according to the nonlinear Bingham plasticity model [17]:

$$\tau=\tau_0(H)\mathrm{sgn}(\dot{\gamma})+\eta\dot{\gamma} \quad |\tau|>|\tau_0| \tag{1}$$

$$\dot{\gamma}=0 \quad |\tau|<|\tau_0| \tag{2}$$

where τ is the MR fluid yield shear stress, τ_0 the yield shear stress caused by the applied magnetic field, H the magnetic field amplitude, η the dynamic viscosity and $\dot{\gamma}$ the shear strain rate. According to the Bingham model, the external shear stress required to activate the MR fluid flow varies in respect of the magnetic field amplitude H. For external shear stress values below to the yield shear stress τ_0 the MR fluid acts like a rigid body.

After the selection of the MR fluid, the materials of the different components were chosen, and design was conducted to develop prototype geometric configuration and electromagnetic circuit characteristics. A FE analysis was required to verify the magnitudes of magnetic induction field B and magnetic field H. The distribution of the magnetic induction field B was observed along the components and the MR fluid to avoid magnetic saturation of the selected MR fluid and materials. The magnetic field H obtained along the gap is used to evaluate the fluid shear stress and the consequent load response, that was estimated by using the analytical formulations for the calculation of the controllable force components F_τ and the viscous force components F_η:

$$F_\tau = \Delta P_\tau A_p = \frac{c\tau_0 L}{h} A_p \tag{3}$$

$$F_\eta = \Delta P_\eta A_p = \frac{12\eta Q L}{h} A_p \tag{4}$$

where ΔP_τ and ΔP_η are the magnetic and viscous pressure drops, A_p is the piston cross sectional area, Q is the MR fluid flow rate, w the average circumference of the narrow gap, h the gap dimension, L the active pole length and v_o the piston speed. The dimensionless parameter c is a function of the pressure drop ratio $\Delta P_\tau/\Delta P_\eta$ and ranges from 2 to 3 [28]

3.2. MR actuator for blankholder control

The actuator geometry and the main components are presented in Fig. 4a. Contrary to the conventional MR damper design, the winding coils of electromagnetic circuit are obtained along an inner annular element. In this way, it is possible to increase both winding coils number and active pole

total length. Consequently, the available force of the MR actuator can be increased, and the overall dimensions kept limited. Due to the alternative piston motion, the MR fluid is forced to flow through the narrow gap obtained by the inner bore and the cylinder, as shown in Fig. 4b. Along the gap, the MR fluid is activated by the magnetic flux generated by the coils, excited by the input currents. Two independent chambers for high-pressure gas are obtained in the piston head and inside the rod, with the aim to pressurize the MR fluid and to allow the returns of the piston at the top dead center after the descending stroke.

The values of the gap and the materials of the components were selected on the basis of FE simulations. Dimensional data and parameters of electromagnetic circuit are reported in Table 1.

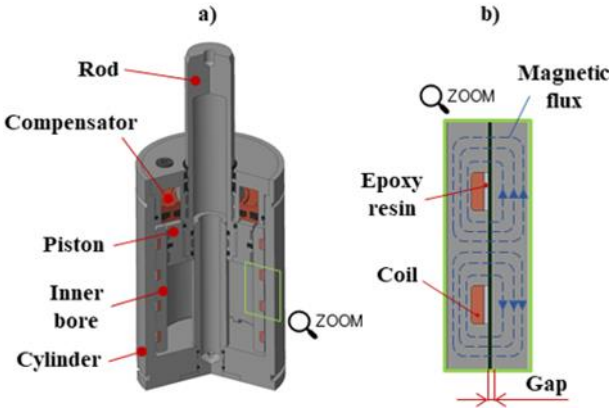

Fig. 4. MR actuator: a) prototype sectional view; b) electromagnetic circuit view.

Table 1. Design parameters of MR actuator.

Parameters	Value
Height	290 mm
External diameter	120 mm
Nominal force	50 kN
Available stroke	75 mm
Wire diameter	0.8 mm
Maximum input current	4 A

3.3. MR fluid

The selected MR fluid is the ARUS AMT-SMARTEC⁺. The main characteristics of this fluids is the capability to achieve high shear yield stress τ_0 when exposed to an external magnetic field H, e.g. for an applied magnetic field amplitude of 140 kA/m, the corresponding MR fluid shear yield stress achieve the value of 69 kPa. Other relevant MR fluid characteristics are reported in Table 2.

According to the specifications provided by the manufacturer, the response time of MR fluid is lower than few milliseconds and the on/off state has high stability, i.e. the change in shear yield stress is totally reversible. To avoid magnetic saturation of the iron particles, disperse in the MR fluid, the maximum admissible magnetic induction field B amplitude does not exceed the value of 1.5 T.

Table 2. Properties of ARUS AMT-SMARTEC⁺.

Parameters	Value
Density	2.90 g/cm^3
Viscosity at 40 °C	0.37 Pa s
Flash point	> 180 °C
Operating temperature range	-20 °C ÷ 150 °C
Solid content by weight	81 %
Shear yield stress at 140 kA/m	69 kPa

3.4. Numerical model and results

To obtain the magnetic field amplitude H as function of the input currents values, the static electromagnetic FE model of the MR prototype is developed using ANSYS Maxwell software. As shown in Fig. 5a, the FE geometry is built as 2D model, resulting in smaller number of nodes and elements. Consequently, the total computation time is contained. This approximation is allowed because both MR device geometry and electromagnetic phenomena that arise within it have axisymmetric configuration.

For an input current of 4 A, the distribution of magnetic saturation field along the materials are presented in Fig. 5b. The material of the inner bore behind the coils have greater sensibility to the magnetic saturation. The inner bore is manufactured of annealed AISI 1040 steel, which has a maximum value of magnetic saturation of 1.8 T. Fig. 5c shows that, for an input current of 4 A, the magnetic field values are 1.7 T at point m_2 and 2 T at m_1 and m_3. As the latter affects only a small region of material, it is possible to apply an input current of 4 A avoiding the magnetic saturation of large region of the inner bore material.

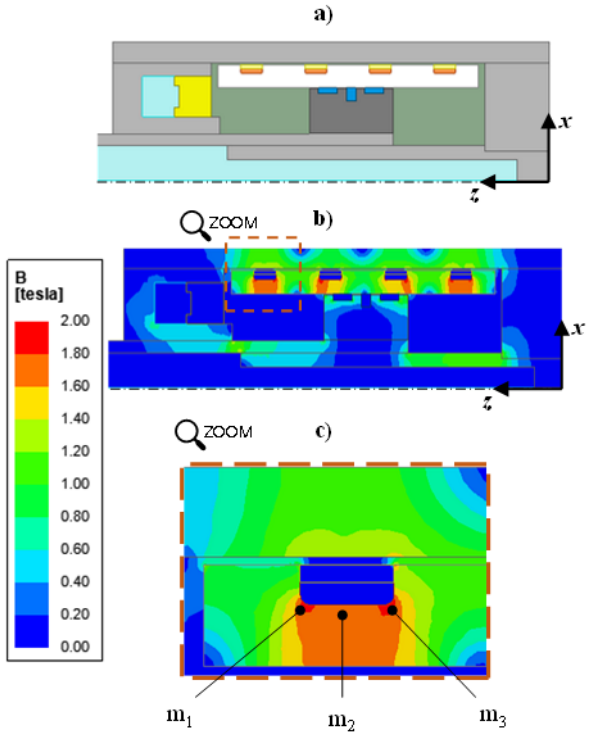

Fig. 5. a) FE model geometry; b) B field; c) B field acting in correspondence of the upper coil.

Fig. 6 presents the trends of magnetic field amplitude along the gap length for different values of input current from 1 A to 4 A. The magnetic field amplitude is low at the extremes of the gap length, resulting in a fall of the average magnetic field amplitude. The MR fluid shear yield stress is obtained from the interpolation of the MR fluid magnetization curve and considering the mean value of each magnetic field distribution of Fig. 6. Thus, the magnetic force F_τ is calculated by mean of Eq. (3), while the viscous force F_η is estimated through Eq. (4), considering geometrical data of the prototype and the properties of MR fluids.

4. Experiments

The prototype was manufactured according to the output from the design phase and then tested on laboratory equipment 50 kN MTS™ dynamometer.

Experimental tests were performed with two values of speed v_0 (namely 50 mm/s and 100 mm/s) and a stroke of 50 mm. Four values of input current, respectively from 1 A up to 4 A with steps of 1 A, as investigated in the numerical model, were used. The two inner chambers of prototype head and rod were filled with nitrogen at initial pressure of 35 bar.

Fig. 7 presents the experimental results in terms of total load of the MR actuator during the performed stroke. The curves associated with the values of 0 A are obtained from tests with null values of the excitation current of the electromagnetic circuit. Therefore, the magnetic force is zero and these curves represent only the viscous force component of the MR actuator. The variation of the curves from 3 A to 4 A is limited due to the modest increase in MR fluid yield shear stress. Consequently, the corresponding variation of magnetic force is limited. For each test, at least two millimeters of initial stroke are required to reach the load associated to a value of excitation current. This initial part of the stroke is used to compress the liquid carrier of MR fluid. After that, the load exerted by the MR actuator remain almost constant, as the experimental curves are horizontal for the entire remaining stroke.

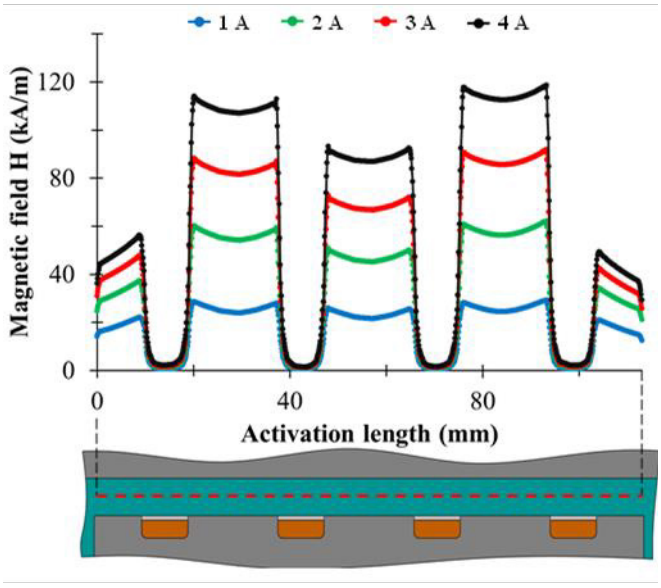

Fig. 6. Magnetic field H magnitude along the gap length for different values of input current.

In Fig. 8, the comparison between experimental and numerical values of magnetic force F_τ is presented for different values of input current. For an input current of 1 A, the experimental values of the magnetic force are almost coincident. For intermediate values of input current (3 A and 4 A), the magnetic force F_τ related to the piston descending velocity of 50 mm/s are slightly higher than the values obtained from test performed at 100 mm/s. This difference is linked to the dependence of the magnetic force on the MR fluid flow conditions, expressed by the coefficient c of Eq. (3). The curves associated with experimental values behave similarly in respect

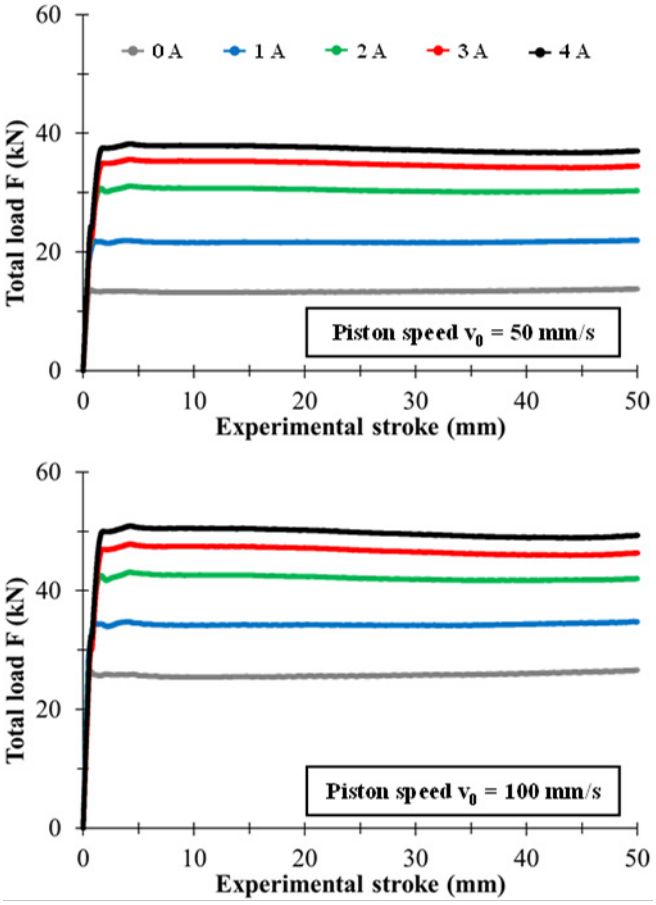

Fig. 7. Total load vs stroke curves obtained from experimental test with two values of piston speed (50 mm/s and 100 mm/s).

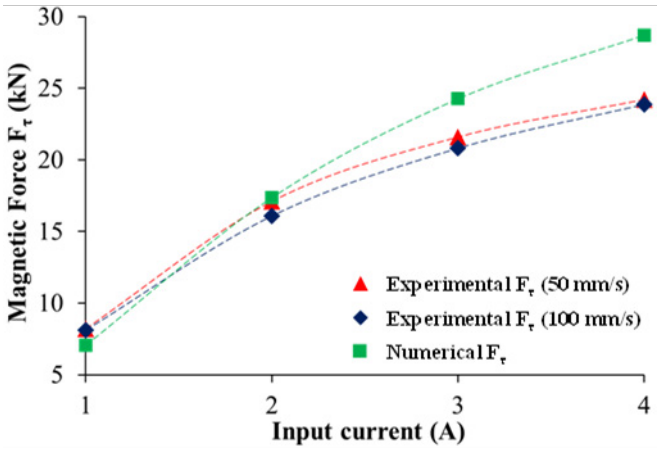

Fig. 8. Magnetic force F_τ experimental and numerical values comparison.

of the numerical values. For an input current of 1 A, both experimental values are slightly higher than the numerical values. This trend reverses in the case of input current of 2 A, and the numerical magnetic force becomes higher than the experimental ones. For greater values of input current, the difference between numerical and experimental magnetic forces arises. This discrepancy can be caused by the occurrence of magnetic saturation of the inner bore material and, indeed, both experimental magnetic forces converge to the same value for the maximum input current of 4 A.

In order to avoid magnetic saturation occurrence, inner bore material has to be replaced with a material with higher magnetic saturation value, e.g. mild steel or soft magnetic alloy.

5. Conclusions

The paper presents the design of a novel MR actuator for active control of blankholder force. The sequence and the main considerations of the design activities are discussed, as well as the FE model and the experimental tests on the manufactured prototype. The results show that numerical and experimental values of magnetic forces are almost in agreement for low input current values. However, for higher values of input current the numerical model overestimates the expected magnetic force and experimental values converge for the maximum input current of 4 A. The occurrence of magnetic saturation in inner bore material for high values of input current is a possible explanation of this behave. Therefore, with the aim to minimize the difference between numerical and experimental forces, inner bore material has to be revised, in order to select a material more suitable for magnetic applications and with higher magnetic saturation values.

References

[1] Gunnarsson L, Asnafi N, Schedin E. In-process control of blank holder force in axi-symmetric deep drawing with degressive gas springs. J Mater Process Technol 1998;73:89-96.
[2] Siegert K, Doege E. CNC Hydraulic Multipoint Blankholder System for Sheet Metal Forming Presses. CIRP Ann - Manuf Technol 1993;42:319–322.
[3] Yagami T, Manabe KI, Yang M, Koyama H. Intelligent sheet stamping process using segment blankholder modules. J Mater Process Technol 2004;155:2099–2105.
[4] Barthau M, Mba HCML. New approach on controlling strain distribution manufactured in sheet metal components during deep drawing process. Procedia Engineering 2017;207:66–71.
[5] Murakawa M, Mo J, Wakatsuki Y, Koga N. Investigation of blanking noise reduction using a hydraulic inertia damper. J Mater Process Technol 2001;112:205–213.
[6] Siegert K, Häussermann M, Haller D, Wagner S, Ziegler M. Tendencies in presses and dies for sheet metal forming processes. J Mater Process Technol 2000; 98: 259–264.
[7] Li R, Bohn ML, Weinmann KJ, Chandra A. A study of the optimization of sheet metal drawing with active drawbeads. J Manuf Process 2000;l:205–216.
[8] Tommerup S, Endelt B, Experimental verification of a deep drawing tool system for adaptive blank holder pressure distribution. J Mater Process Technol 2012;212:2529–2540.
[9] Endelt B, Tommerup S, Danckert J. A novel feedback control system - Controlling the material flow in deep drawing using distributed blank-holder force. J Mater Process Technol 2013;213:36–50.
[10]Baume T, Zorn W, Drossel WG, Rupp G. Step by step control of a deep drawing process with piezo-electric actuators in serial operation. MATEC Web Conf 2015;21.
[11]Bäume T, Zorn W, Drossel WG, Rupp G. Iterative process control and sensor evaluation for deep drawing tools with integrated piezoelectric actuators. Manuf Rev 2016;3:1–8.
[12]Siegert K, Ziegler M, Wagner S. Closed loop control of the friction force. Deep drawing process. J Mater Process Technol 1997; 71: 126–133.
[13]Mahayotsanun N, Sah S, Cao J, Peshkin M, Gao RX, Tao Wang C. Tooling-integrated sensing systems for stamping process monitoring. Int J Mach Tools Manuf 2009;49:634–644.
[14]Maier S, Liebig A, Kautz T, Volk W. Tool-integrated spring back measuring system for automotive press shops: A contribution to the quality control of complex car body parts. Prod Eng 2017;11:307–313.
[15]Gao RX, Sah S, Mahayotsanun N. On-line measurement of contact pressure distribution at tool-workpiece interfaces in manufacturing operations. CIRP Ann - Manuf Technol 2010;59:399–402.
[16]Groche P, Brenneis M. Manufacturing and use of novel sensoric fasteners for monitoring forming processes. Meas J Int Meas Confed 2014;53:136–144.
[17]Yang G, Spencer BF, Carlson JD, Sain MK. Large-scale MR fluid dampers: Modeling and dynamic performance considerations. Eng Struct 2002;24:309–323.
[18]Parlak Z, Engin T, Çalli I. Optimal design of MR damper via finite element analyses of fluid dynamic and magnetic field. Mechatronics 2012;22:890–903.
[19]Lam KH, Chen ZH, Ni YQ, Chan HLW. A magnetorheological damper capable of force and displacement sensing. Sensors Actuators A Phys 2010;158:51–59.
[20]De Jesus Lozoya-Santos J, Sename O, Dugard L, Morales-Menendez R, Ramirez-Mendoza R. A semi-active control-oriented damper model for an automotive suspension. IFAC Proceedings Volumes 2010;43:336–341.
[21]Yerrawar RN, Arakerimath RR. Development of Methodology for Semi Active Suspension System Using MR Damper. Materials Today: Proceedings 2017;4:9294–9303.
[22]Park EJ, da Luz LF, Suleman A. Multidisciplinary design optimization of an automotive magnetorheological brake design. Comput Struct 2008;86:207–216.
[23]Karakoc K, Park EJ, Suleman A. Design considerations for an automotive magnetorheological brake. Mechatronics 2008;18:434–447.
[24]Hema Latha K, Usha Sri P, Seetharamaiah N. Design and Manufacturing Aspects of Magneto-rheological Fluid (MRF) Clutch. Materials Today: Proceedings 2017;4:1525–1534.
[25]Lanzotti A, Renno F, Russo M, Russo R, Terzo M. Design and development of an automotive magnetorheological semi-active differential. Mechatronics 2014;24:426–435.
[26]Ghiotti A, Regazzo P, Bruschi S, Bariani PF. Reduction of vibrations in blanking by MR dampers. CIRP Ann - Manuf Technol 2010;59:275–278.
[27]Ghiotti A, Bruschi S, Regazzo P. Shear surface control in blanking by adaptronic systems. Procedia Eng 2014;81:2512–2517.
[28]Jolly MR, Bender JW, Carlson JD. Properties and Applications of Commercial Magnetorheological Fluids. J Intell Mater Syst Struct 1999;10:5–13.